Micro-meso draping modelling of non-crimp fabrics

Oleksandr Vorobiov[1], Dr. Th. Bischoff[1], Dr. A. Tulke[1]

[1]FTA Forschungsgesellschaft für Textiltechnik mbH

1 Introduction

Non-crimp fabrics (NCFs) are widely used in the composite materials as a reinforcement part due to a combination of both high mechanical properties in main fibre directions and better handling compared to UD tapes. For prediction of mechanical response of composite parts in particular with high curvature it is important to consider the local orientations and gaps in textile structures obtained after draping. For this goal the simulations on the textile structure scale (meso-scale) are commonly used.
In the present work the new approach for the modelling of the textile structures is proposed. In this approach the mechanical properties of the textile yarns are obtained from the micro-scale simulations of the glass roving. This allows to investigate the dependency to the fibre volume fraction (FVFr) of the roving. Although micro-scale modelling as the basis for textile simulations was used in [1], but only small micro-models without taking into account the cross-section change during the compaction was investigated. Latter can play a major role in forming processes like RTM.
The representative volume element (RVE) of the structure should be generated without the interpenetrations, which is hardly possible for geometrical generation especially for the complex textile structures such as NCFs [2]. New method for the generating of the free of interpenetrations RVE based on the thermal expansion in transverse direction was proposed.
The other aspect of the composite simulations is the prediction of the mechanical properties. Commonly used method where the textile geometry is subtracted from the matrix is causes bad quality mesh of the model or fails at all. For this reason the mesh superposition (MSP) [3, 4] technique is preferable for investigating of the stiffness behaviour. In present work this was implemented in LS-Dyna.

2 Micro-modelling of the roving

Generally the roving can be described as a transverse isotropic material with axis of symmetry on the roving length axis. There are six main deformation modes: length tension and compaction, transverse tension and compaction, shear and torsion.
In this work following assumptions are made:

- compression stiffness in length direction as well as tension stiffness in transverse direction of the roving is negligible;
- length stiffness of the roving has a linear dependency only on FVFr and may be calculated due to mixture rule like $E_l = \theta \cdot E_{l\,f}$, where θ is the FVFr and $E_{l\,f}$ is a filament elastic modulus;
- there is no significant strain in transverse direction due to length deformation, so the poisson's ratio $\eta_{lt} = 0$;
- fibre-fibre friction is assumed to be constant.

The constitutive law of the roving material in this case may be written as follows:

$$\begin{bmatrix} \varepsilon_x \\ \varepsilon_y \\ \varepsilon_z \\ \varepsilon_{xy} \\ \varepsilon_{yz} \\ \varepsilon_{xz} \end{bmatrix} = \begin{bmatrix} 1/(\theta \cdot E_{l\,f}) & 0 & 0 & 0 & 0 & 0 \\ 0 & 1/E_t(\theta) & -\eta_{tt}(\theta)/E_t(\theta) & 0 & 0 & 0 \\ 0 & -\eta_{tt}(\theta)/E_t(\theta) & 1/E_t(\theta) & 0 & 0 & 0 \\ 0 & 0 & 0 & 1/(2G_{tl}(\theta)) & 0 & 0 \\ 0 & 0 & 0 & 0 & 1/(2G_{tt}(\theta)) & 0 \\ 0 & 0 & 0 & 0 & 0 & 1/(2G_{tl}(\theta)) \end{bmatrix} \cdot \begin{bmatrix} \sigma_x \\ \sigma_y \\ \sigma_z \\ \sigma_{xy} \\ \sigma_{yz} \\ \sigma_{xz} \end{bmatrix} \quad (1)$$

This means that we need to define four constants that should depend non-linear on the FVFr θ.

2.1 Used models

For determination of the missing mechanical properties, quasi-static FE simulations on micro-scale were performed. Used models for different load cases are presented on the Figure 1.

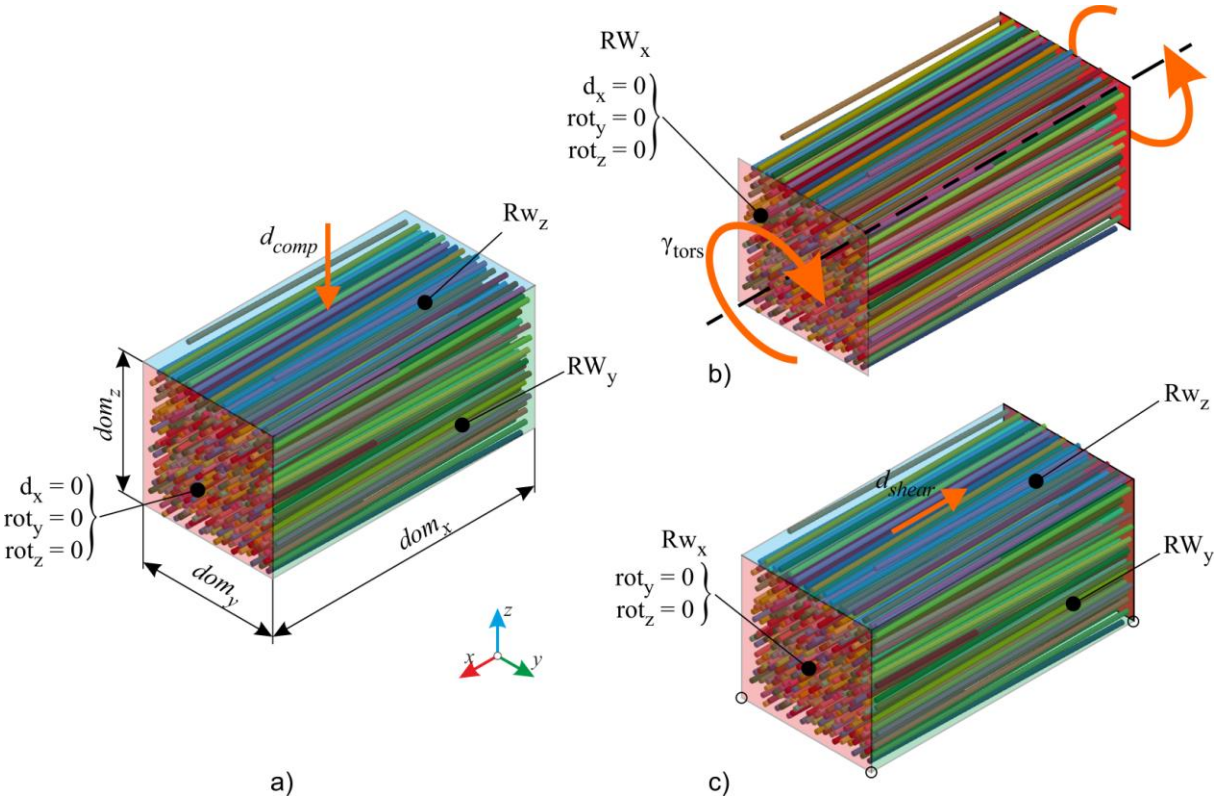

Fig.1: Roving models used for micro-simulations: (a) transverse compaction, (b) torsion and (c) shear loading cases.

The mechanical properties of the filaments were taken from the data sheet of the glass roving, which was used for manufacturing of the leno-woven NCFs. The diameter of one filament is $d_f = 17\mu m$, density $\rho_f = 2.62\, g/cm^3$, isotropic elastic modulus $E_f = 82GPa$ with poisson's ratio $\eta_f = 0.2$. Friction coefficient for fibre-fibre contact was chosen to be 0.3.

The filaments in the roving have some degree of misalignment due to the manufacturing processes of the textile and roving itself. In this work this effect was investigated by performing the simulations for various standard deviations of the filament angle.

The structures were generated with GeoDict software [5] and then these models were transferred to LS-Dyna a converter software with developed in FTA [6]. These models have about 600 filaments inside of the domain of 1x0.5x0.5 mm³ for dom_x, dom_y and dom_z respectively. Initial FVFr of the models was about 25% depending on the standard deviation of the filament orientations.

To ensure the contact, each filament is represented as a sequence of High-Liu beams with length of $l_{fb} = 2 \cdot d_f = 34\mu m$. Rigid walls (RW) are generated on the sides of the domain. Periodicity in length direction was implemented through restriction of displacement in x-directions as well as rotations along y and z axis for nodes, that lie on the domain x face.

2.2 Transverse compaction

The general model for transverse compaction is represented at Figure 1 a. The roving is compressed in z direction so as the final FVFr would be $\theta_f \approx 0.85$.

The upper RW_z compresses the roving, while other three remain stationary. This approach allows to investigate on one loading case both the compression stiffness and the expansion effect in other transverse direction (*y*), which is non-linear and may be significant for higher FVFrs.

The pressure versus FVFr dependency for both *z* and *y* directions is shown in Figure 2. It may be seen, that the basic shape of the curves remains the same with shifting to small FVFr when the filament misalignment increases. Both *y* and *z* pressures start to increase at the same FVFr.

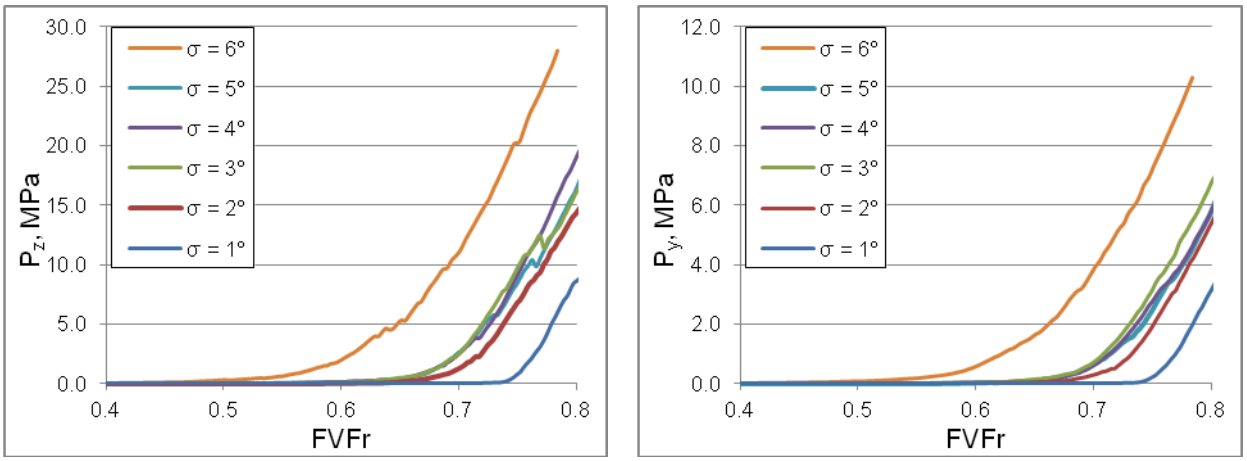

Fig.2: Pressure in compression- and transverse directions of the roving on micro-scale for different standard deviations of the filaments orientations.

Further, the poisson's ratio and transverse elastic modulus may be expressed through the RW pressure values as follows:

$$\eta_{tt}(\theta) = P_y / P_z \,;\; E_t(\theta) = \left(P_z - \eta_{tt} \cdot P_y\right) / \varepsilon_z \,, \tag{2}$$

where ε_z is the logarithmic strain in compaction direction.

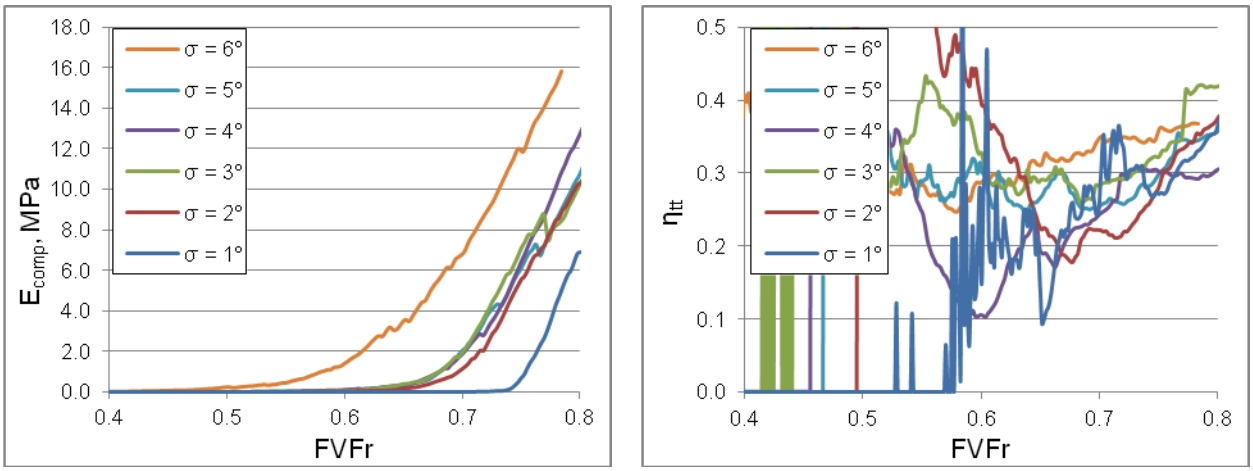

Fig.3: Elastic modulus and poisson's coefficient of the roving on micro-scale for different standard deviations of the filaments orientations.

The shape of the E_{comp} curve remains smooth, while the poisson's tends to oscillate (Figure 3). It can be solved by using the models with higher amount of filaments inside and thus bigger domain dimansions. Still with used models the general trends of increasing of the poisson's ratio with increasing of the FVFr. The slope of the curve decreases with increasing of the filament misalignment. Model results were written out during the solution for FVFr of 0.5, 0.6, 0.7 and 0.8 for further torsion and shear calculations.

2.3 Torsion

The torsion of 10° is applied to the roving as shown on the Figure 1 b. The shear modulus is then computed as follows:

$$G_{tt}(\theta) = \frac{2 \cdot E_{\text{int}} \cdot dom_x}{J \cdot \gamma^2} \,, \tag{3}$$

where E_{int} is the internal energy of the roving, γ - torsion angle and J is a polar area moment of inertia.

Results for different FVFr and filament misalignments with standard deviation of 1° and 4° are presented in the Figure 4. It may be seen, that with increasing of the FVFr and torsion angle the shear modulus in the tt-plane increases.

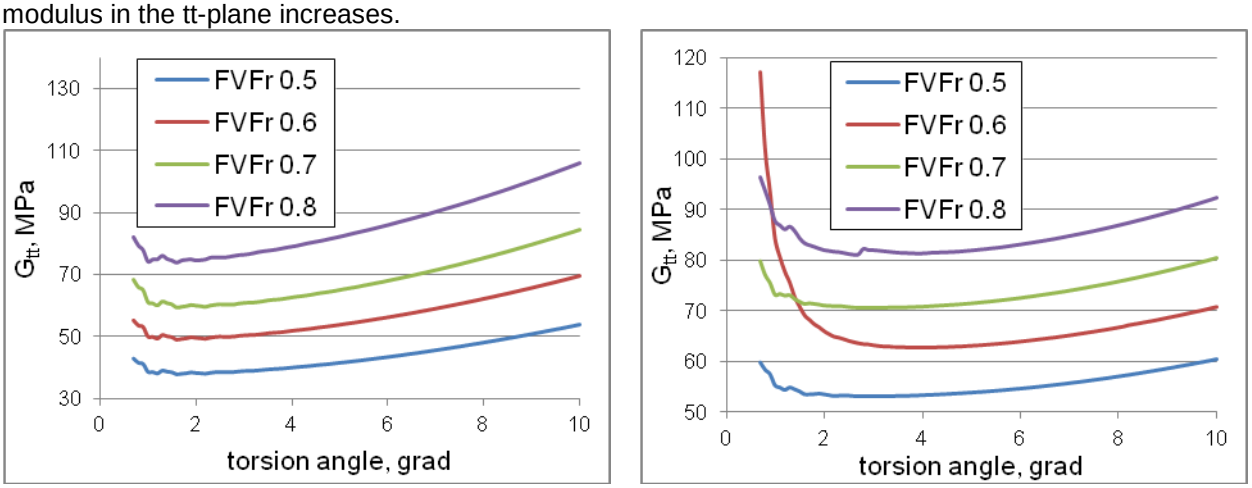

Fig.4: Shear modulus G_{tt} versus torsion angle for a) 1° standard deviation of the filament orientation and b) 4°.

2.4 Shear

For the same models the shear simulations for determination of the shear modulus G_{lt} were performed (Figure 1 c). Obtained shear modulus for standard deviation of 1° and 4° are represented in the Figure 5.

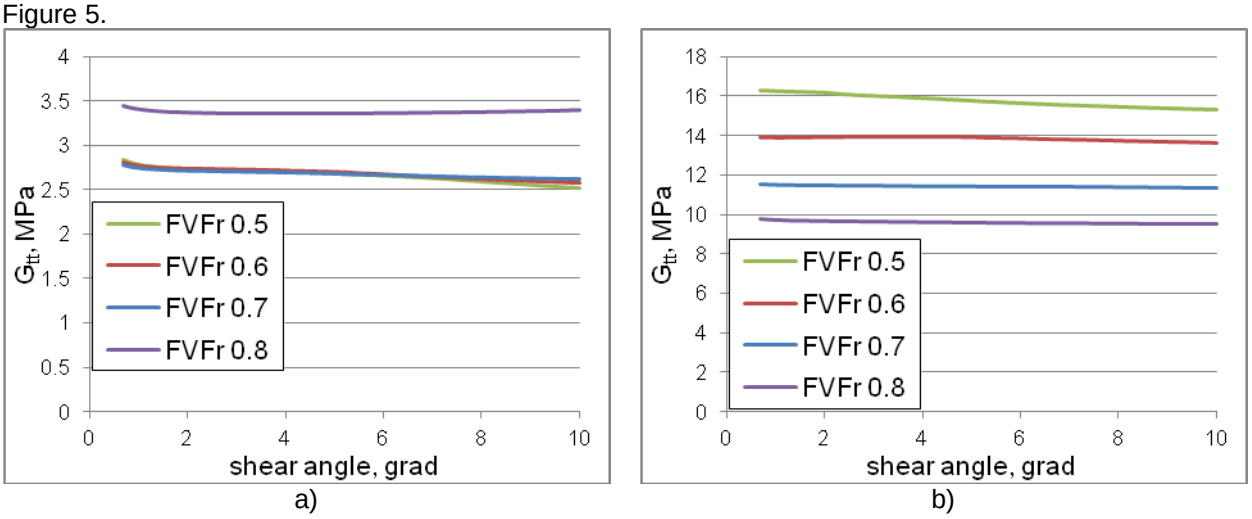

Fig.5: Shear modulus G_{lt} versus shear angle for a) 1° standard deviation of the filament orientation and b) 4°.

In this case it may be seen, that the shear modulus G_{lt} doesn't change with the shear angle. As well as the trend to decreasing of the stiffness with increasing of the FVFr may be observed. This effect should be investigated in further studies.

3 Implementation of user defined material model

The FVFr of the element may be obtained at each iteration as follows:

$$\theta = \theta_0 / \exp(\varepsilon_t) = \theta_0 / \exp(\varepsilon_2 + \varepsilon_3), \quad (4)$$

where θ_0 is the initial FVFr of the element and ε_2 and ε_3 are the complete strains in the 2 and 3 directions respectively.

The elastic modulus obtained from micro-scale simulation may be approximated with the power law as described in [1]. The poisson´s ratio is also assumed to be approximated with power law. The shear modules are linear dependent from the FVFr:

$$E_t = A_E \cdot \theta^{B_E}; \eta_{tt} = A_\eta \cdot \theta^{B_\eta}; G_{tt} = A_t \cdot \theta + B_t; G_{lt} = A_l \cdot \theta + B_l, \quad (5)$$

where the A and B are constants for different mechanical properties obtained from the micro-simulations of the roving.

4 Generation of the RVEs

For the generation of the RVE the thermal expansion in the transverse direction of the rovings was used. It allows generating the complex textile structures without interpenetrations and use them for various simulations. The user defined material model described above was assigned to yarns. This allows to consider the local FVFr and real compression / shear behaviour.
The dirichlet periodic boundary conditions (BC) were applied to the ends of the each yarn to estimate the periodicity of the obtained structure. Although the length of the auxiliary yarns was taken from the measurements on the real textile.
Different RVE should be used for draping and mechanical simulations. From one hand, in the draping simulations the big areas of the textile should be modelled, so the model simplification plays very important role. The auxiliary yarns may be represented as beam elements and only two solid elements in thickness directions of the reinforcement yarns should be used. On the other hand, in mechanical simulations also the stress distributions inside of the auxiliary yarns and close to them may play a role, so more refined RVE is preferable. For this case the true shape of the yarns should be considered.

4.1 Draping simulation

The initial textile structure with rescaled cross-sections of the yarns is shown in the Figure 6. The auxiliary yarns in the initial condition have the circle cross-section and for preserving of the cross-section change during the thermal expansion simulation, the material MAT_022 was used with high transverse and length modules ($E_1 = E_2 = E_3$) but remaining the shear modules on the roving level. Different scale factors ($sf = d_{init}/d_{real}$) were used.

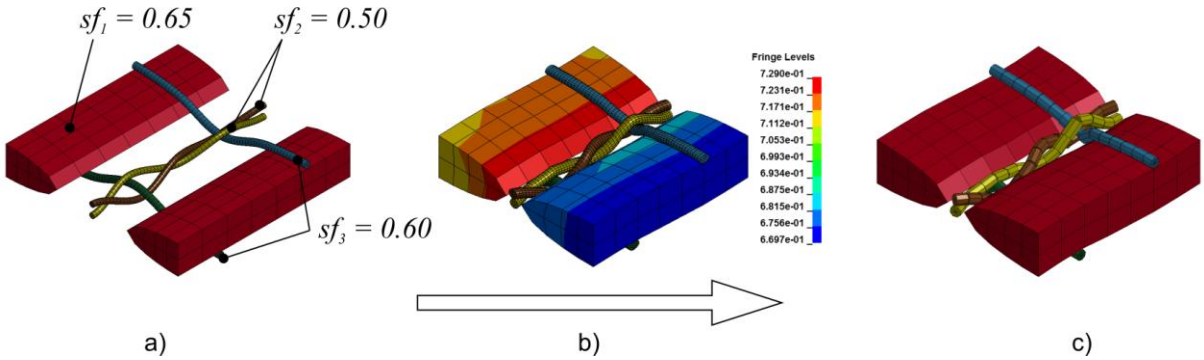

Fig.6: RVE of the leno-woven NCF for draping simulation: a) initial conditions, b) after thermal expansion simulation with calculated local FVFrs and c) auxiliary yarns are represented as beams.

Obtained structure consists only of 112 solid elements and 60 beam elements with dimensions of RVE 4 x 4 cm².

4.2 Calculation of the mechanical properties

In real structure the auxiliary yarns have an elliptical cross-section. This should be considered in the initial configuration, what yields to smaller initial cross-sections. For obtaining the desired composite thickness, the rigid walls on the top and the bottom of the structure are generated (Figure 7).

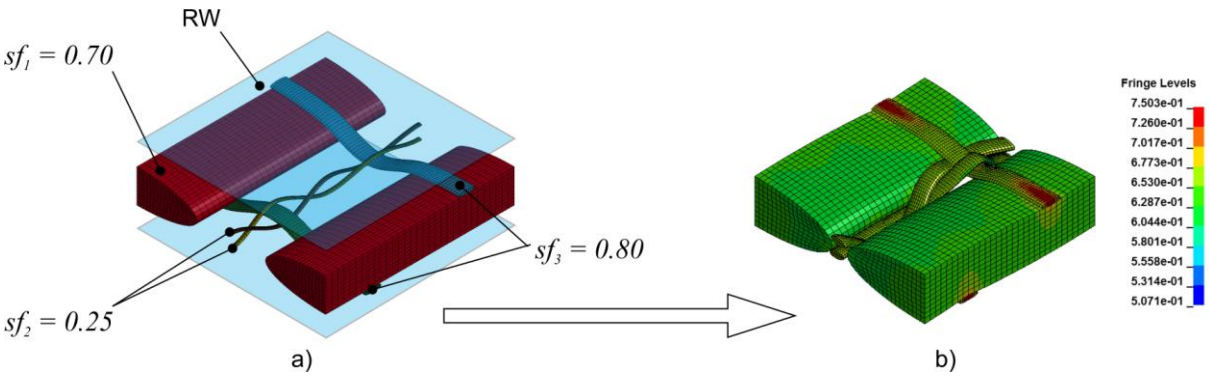

Fig.7: RVE of the leno-woven NCF for calculation of the mechanical properties: a) initial conditions, b) after thermal expansion simulation with calculated local FVFrs.

The cross-section of the generated structure conforms to the microcut image of real textile like shown in the Figure 8.

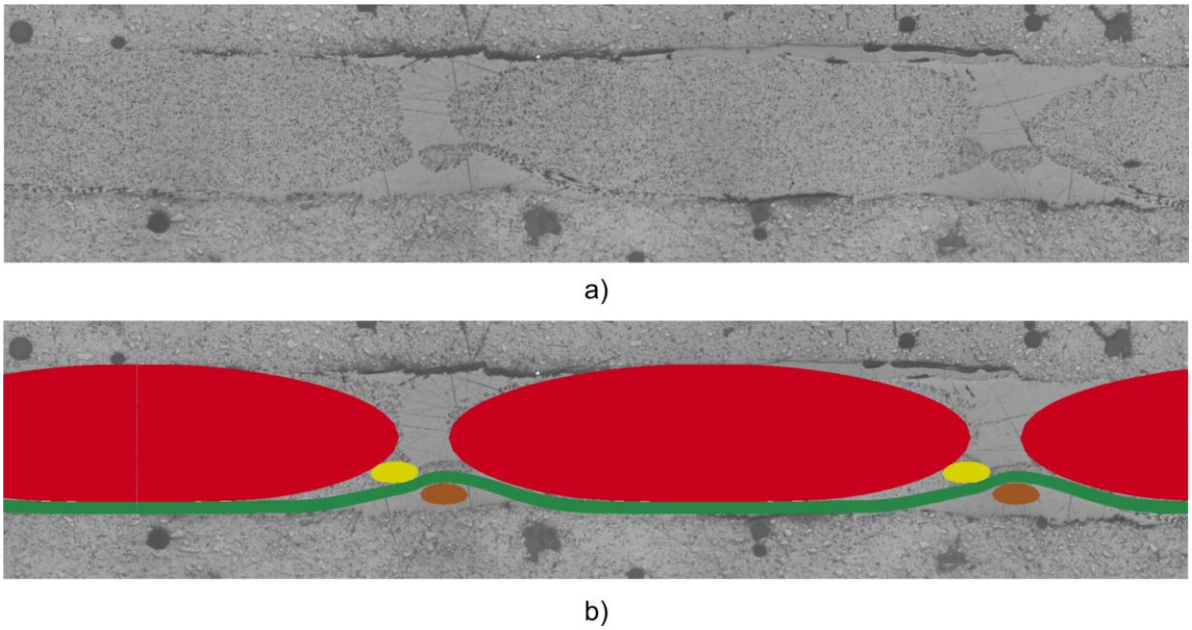

Fig.8: Microcut image of the glass leno-woven NCF composite (a) and comparison with the simulation section view (b).

5 Validation of the developed model

5.1 Single roving compaction

For validation purposes, the following experiment set-up was used (Figure 9 a). It consists of two plates with the lower one is made of transparent material. A camera is located underneath, which is needed to record the width change during the compaction.

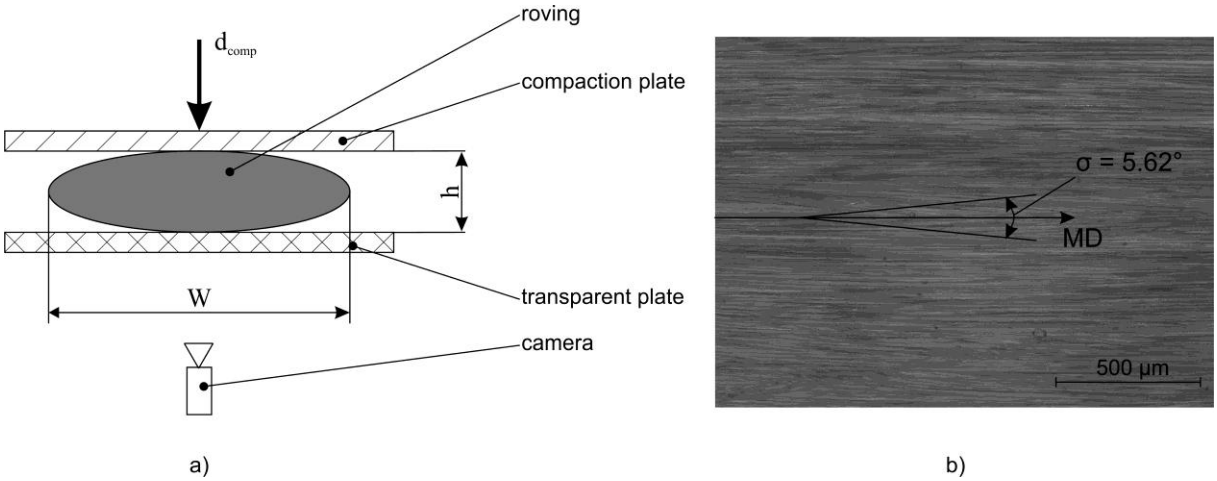

Fig.9: Roving compaction: a) experimental stand, b) roving outer surface.

For estimation of the required parameters of the developed material model, the filament orientation distribution is necessary. For this purpose the outer surface of rovings taken from leno-woven NCF was microscopically investigated and the mean and standard deviation values were calculated (Figure 9 b). For this structure the average standard deviation value of the filament misalignment was $\sigma = 5.5°$.

The values of the transverse compaction elastic modulus and poisson's ratio were averaged between $\sigma = 5°$ and $\sigma = 6°$. The approximation with a power function is shown in Figure 10.

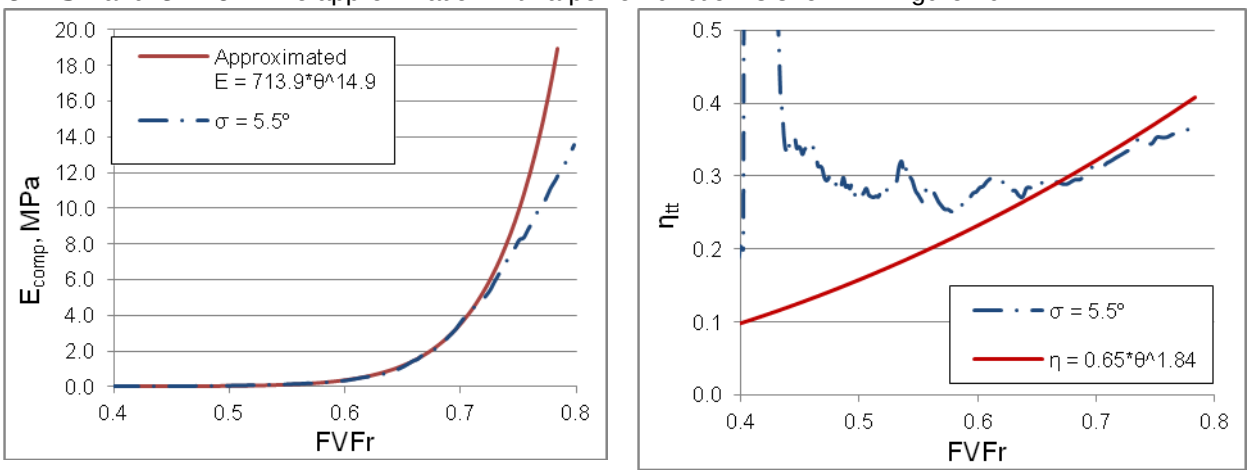

Fig.10: Material parameters used for roving simulations: a) elastic modulus and b) poisson's ratio.

The simulation results are showing good agreement with experimental results without some extra tuning of the parameters as it is shown on the Figure 11. Although some small deviations may be observed. These may be the reason of using relative small models for micro-simulations as discussed above.

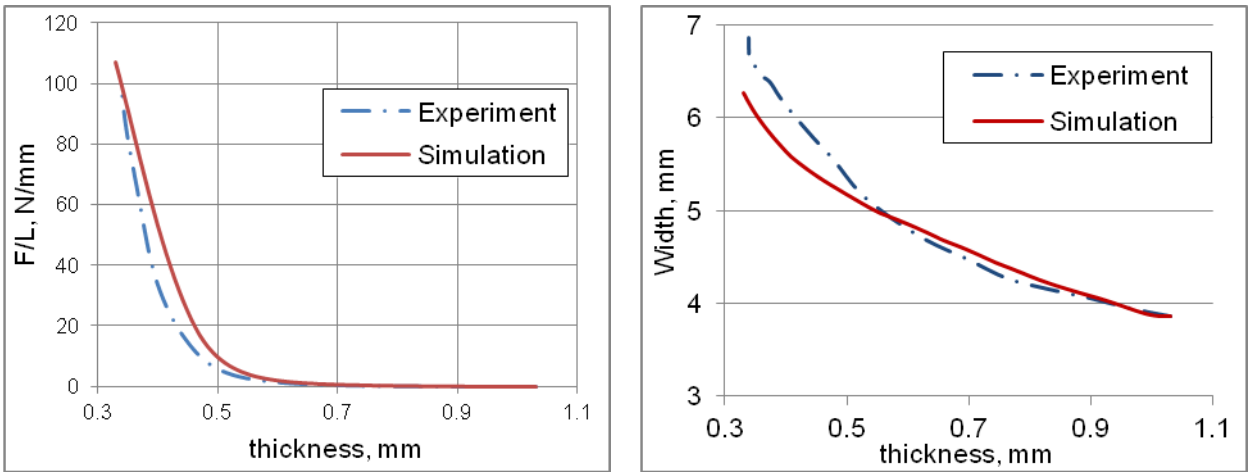

Fig.11: Comparison of the experimental and simulation results for roving compaction: a) compaction force per unit length and b) roving width versus roving thickness.

5.2 Stiffness of the composite

The RVE described in Section 4.2 was used for prediction of the mechanical properties of the composite. For coupling of the textile reinforcement to the matrix the MSP technique was used. It was implemented in LS-Dyna by using of the **`*CONSTRAINED_MULTIPLE_GLOBAL`** keyword and placing the nodes of the textile mesh as first in the assignment. The same keyword was used to apply the dirichlet periodical BC to the matrix faces. Simulations for all six load cases with implicit iterative solver were performed and then homogenized mechanical properties were compared with experimental in the Table 1. Maximal error lies below 4%.

Mechanical property	Experiment	Simulation	Error
E_x, GPa	37,7 ± 0,55	36,7	-2,7%
E_y, GPa	10,5 ± 0,20	10,9	3,8%
G_{xy}, GPa	-	3,7	
μ_{xy}	0,25	0,33	
μ_{yx}	0,087	0,10	

Table 1: Mechanical properties of the composite based on leno-woven UD NCF.

5.3 Drapeability

Described in Section 4.1 RVE of leno-woven NCF was used to perform the drapeability simulation (Figure 12). Due to the symmetry only one fourth of the model was built with the textile diameter of 330 mm.

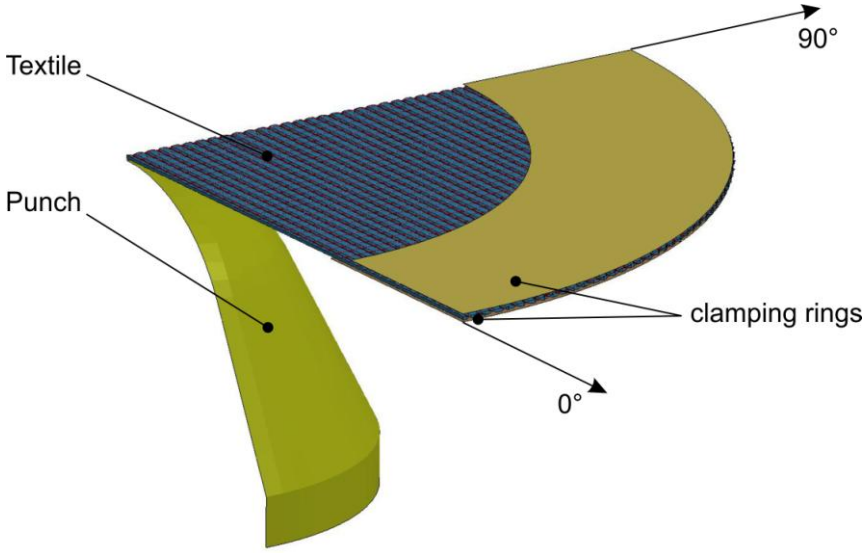

Fig.12: Model for the draping simulation.

In considered test, the punch drives until 80 mm into the fabric from underneath and at steps of 10 mm the force of the punch is taken as well as the pictures of textile on several positions.
Total punch force calculated within simulation shows very good agreement with test results (Figure 13).

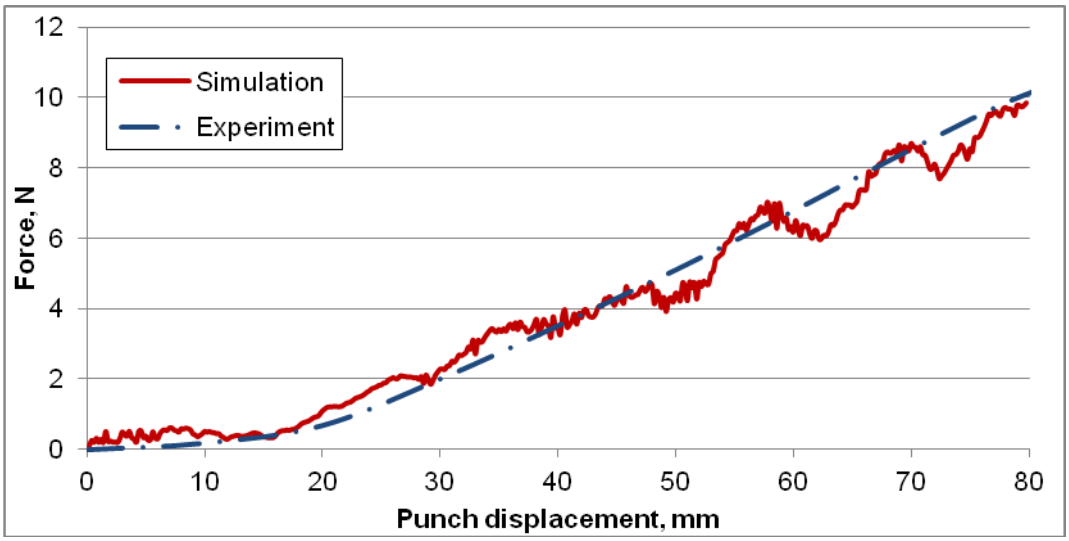

Fig.13: Punch force versus punch displacement obtained from simulation and experiment.

The pictures of the textile structure at the highest punch location are compared in the Figure 14. Both experiment and simulation are showing very small amount of gaps at 0° and 45° whereas at 90° the DRAPETEST shows more local gaps which are not observed in simulation results.

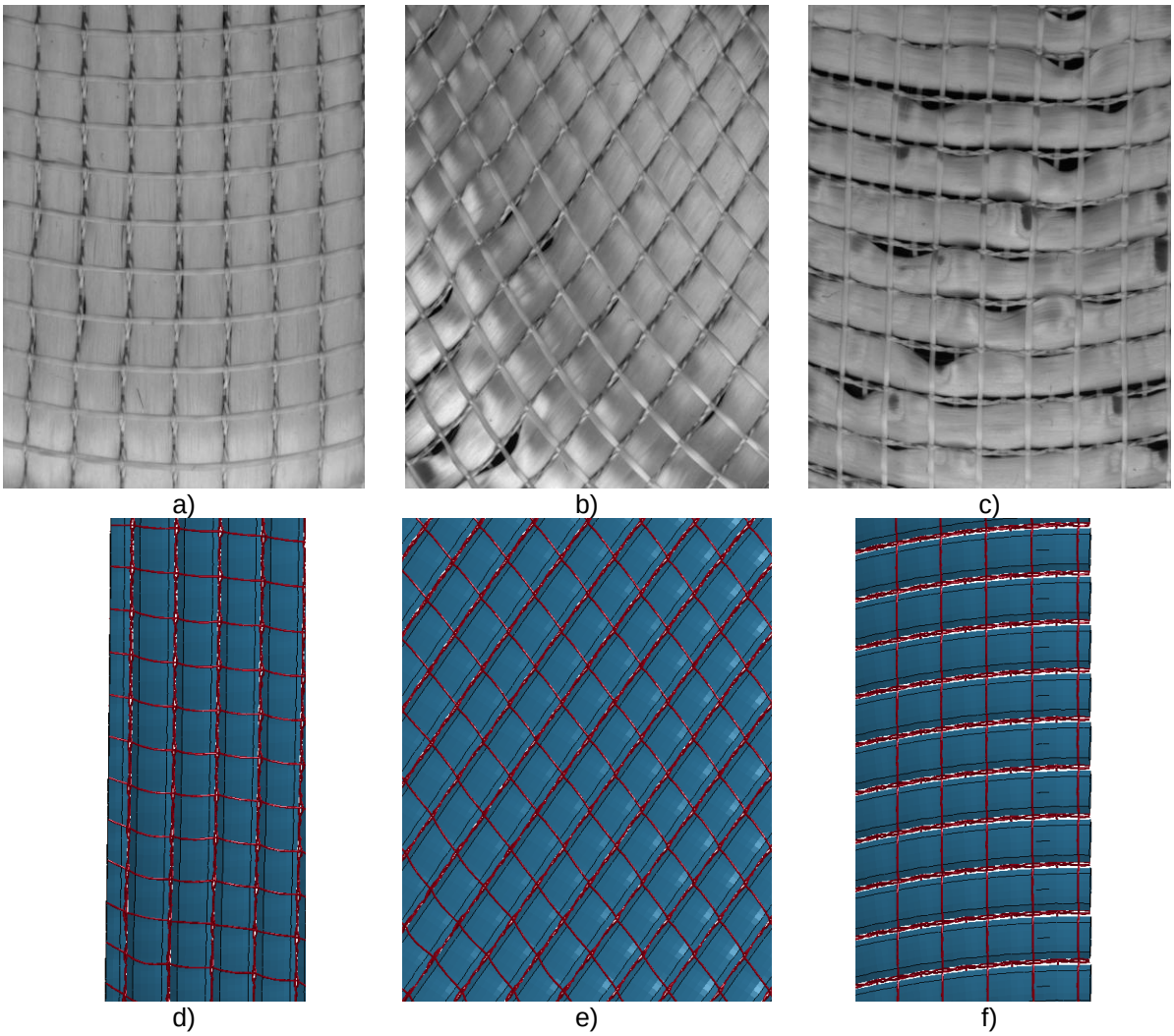

Fig.14: Textile pictures taken from the DRAPETEST camera at the punch displacement 80 mm on a) 0°, b) 45° and c) 90° and at the corresponding positions from simulation d – f.

The contour of the textile after draping made with the camera on the top of the DRAPETEST has very good agreement with the simulation results (Figure 15).

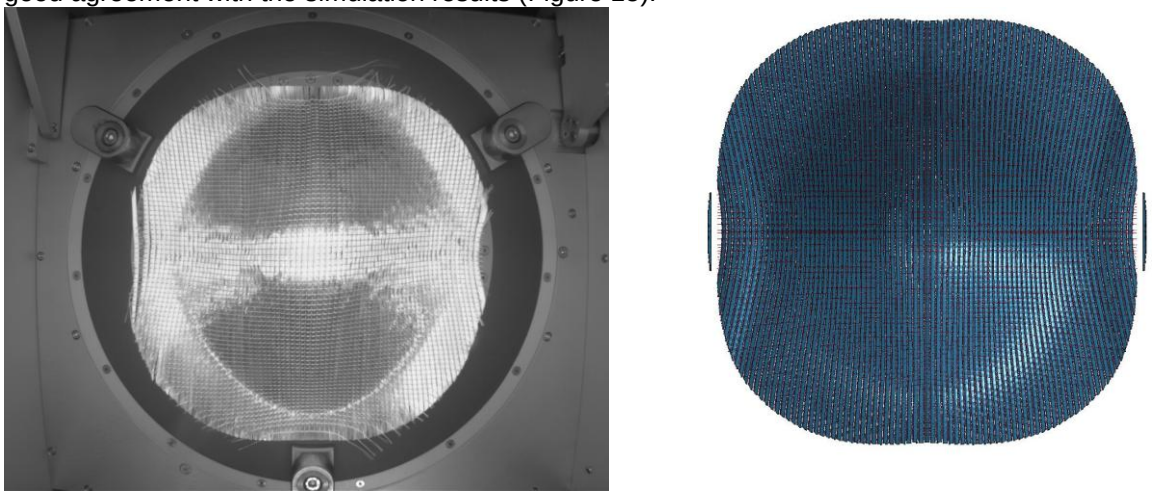

Fig.15: Textile shape after draping: a) DRAPETEST and b) simulation.

6 Summary

In the present work a novel approach for modelling of the reinforcement NCFs was proposed. For estimating of the mechanical behaviour of the textile yarns the microscopic simulations of the roving with different levels of filament misalignments were performed. Obtained properties were direct transferred in the developed user material model and without any parameter tuning very good agreement with experimental results of simple roving compaction was reached both for compression force and cross-section shape change. This material model was also used for generating of the RVE using thermal expansion method of glass leno-woven NCF for different scales of refinement. The drapeability of the textile structure was validated based on drapeability tester called DRAPETEST by Textechno. The forming force converges very well with the measured experimentally. Also the deformation of the textile has the same character. This model may be useful also in simulations of other forming processes like RTM, where the cross-section changes may be significant. MSP method for calculation of the mechanical properties of textile reinforcement composite was implemented in LS-Dyna. This method gave the error below 4% comparing to the experimental results.

7 Literature

[1] Sherburn M., “Geometric and Mechanical Modelling of Textiles”, PhD thesis, 2007

[2] Lomov S.V., Ivanov D.S., Verpoest I., Zako M., Kurashiki T., Nakai H., Hirosawa S., "Meso-FE modelling of textile composites: Road map, data flow and algorithms," *Composites Science and Technology*, no. 67, pp. 1870-1891, 2007.

[3] Tabatabaei S.A., Lomov S.V., Verpoest I., "Assesment of embedded element technique in meso-FE modelling of fibre reinforced composites," *Composite structures*, no. 107, pp. 436-446, 2014.

[4] Jiang WG, Hallett SR, Wisnom M., "Development of domain superposition technique for the modelling of woven fabric composites," in *Mechanical response of composites*.: Springer, 2008.

[5] www.geodict.com

[6] O. Vorobiov: "Interfacing GeoDict Analytical Data to LS-Dyna and ANSYS", GeoDict User Meeting 2014, Kaiserslautern, 2014